Journal Pre-proof

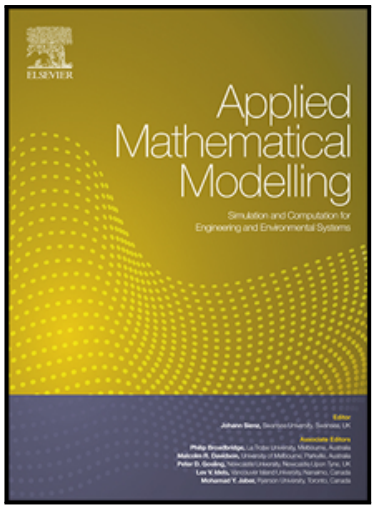

A fully Eulerian multiphase model of windblown sand coupled with morphodynamic evolution: erosion, transport, deposit and avalanching

A. Lo Giudice, L. Preziosi

PII: S0307-904X(19)30481-0
DOI: https://doi.org/10.1016/j.apm.2019.07.060
Reference: APM 12967

To appear in: *Applied Mathematical Modelling*

Received date: 21 December 2018
Revised date: 10 May 2019
Accepted date: 25 July 2019

Please cite this article as: A. Lo Giudice, L. Preziosi, A fully Eulerian multiphase model of windblown sand coupled with morphodynamic evolution: erosion, transport, deposit and avalanching, *Applied Mathematical Modelling* (2019), doi: https://doi.org/10.1016/j.apm.2019.07.060

Highlights

- A comprehensive mathematical model for windblown sand transport and morphodynamics evolution of the sand bed is presented
- The model takes into account suspension in the air, saltation, erosion, deposition, turbulent diffusion and avalanching
- Local slope modifies shear-velocity threshold: a 3D correction factor is proposed to include this effect
- Numerical simulations of both dunes evolution and windblown sand around mitigation measures are performed
- The transport process is correctly reproduced in both cases

A fully Eulerian multiphase model of windblown sand coupled with morphodynamic evolution: erosion, transport, deposit and avalanching

A. Lo Giudice[1,2,3,*], L. Preziosi[1,3]

[1] *Dept. Mathematical Sciences, Dipartimento di Eccellenza 2018-2022, Politecnico di Torino, Corso Duca degli Abruzzi 24, Torino, I-10129, Italy*
[2] *Optiflow Company, 160 Chemin de la Madrague-Ville, F-13015, Marseille, France*
[3] *WSMM - Windblown Sand Modeling and Mitigation Joint Research Group*

Abstract

Modelling unsteady windblown sand dynamics requires not only to treat the sand present in the air as a suspended constituent of a mixture, but also to take care of erosion and sedimentation phenomena and consequently of the morphodynamic evolution of the sand-bed surface, including avalanching, especially in presence of natural or human built obstacles, artifacts, and infrastructures. With this aim in mind, we present a comprehensive multiphase model capable of accurately simulating all the physical phenomena mentioned above, producing satisfactory results, with a reasonable computational effort. As case tests, two- and three-dimensional simulations of dune evolution are reported, as well as windblown sand transport over a straight vertical wall. Example of the sand transport around other obstacles are given to show the flexibility of the model and its usefulness for such engineering applications.

Keywords: Windblown sand, Multiphase flow, Morphodynamics, Transport phenomena

1. Introduction

When wind blowing on a sandy surface, like a beach or a dune in the desert, is sufficiently strong, sand particles are set in motion from the sand-bed and entrained in the air flow. Depending on their diameter, sand grains are then transported due to different physical mechanisms: bigger grains start to roll (creep), medium size grains describe ballistic-like trajectories and impact again on the

sand surface triggering a chain reaction by colliding with other particles, a phenomenon known as saltation, while smaller grains are entrained by the wind forming a very thin suspension that can transport sand dusts over large distances (see Fig. 1). Among the cited transport mechanisms, saltation involves almost 80% of the total moving mass [1]. By sedimentation, then, sand grains accumulate in new downwind regions and pile up until the sand-bed surface reaches a slope that exceeds a critical repose angle. Above this angle avalanching occurs redistributing the sedimented mass so that a new stable configuration is established. In order to model this quite complex physical phenomenon, it is crucial to consider all the aspects mentioned above. The aim of this work is then to present a comprehensive mathematical and computational model capable to accurately simulate windblown sand transport, taking into account of sand erosion, grains entrainment in the wind flow, deposition, and avalanches determining the morphodynamic evolution of the sand bed.

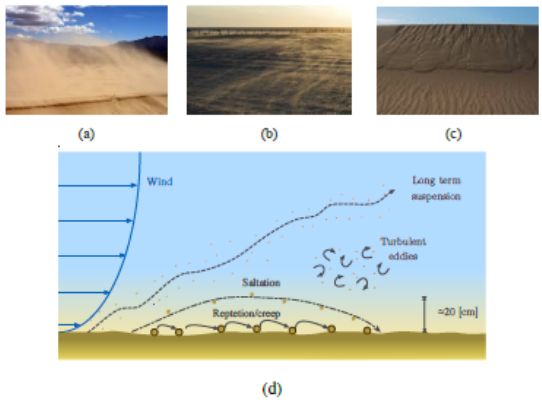

Figure 1: Sand transport and morphodynamic evolution: a) erosion and suspension, (b) saltation, (c) avalanching (d) schematization of transport mechanisms.

Historically speaking, Bagnold [2] paved the way for the scientific investigation of windblown sand. However, only recently computational approaches have taken hold even if some early attempts have been done in the eighties (see for instance [3]). Then, with the aim of modelling the motion of dunes, several authors (see, for instance, [4, 5, 6, 7, 8, 9]) have proposed models for sand transport, most of them using perturbation theories and linearizations to evaluate wall-shear stress, but without using multiphase coupling.

With respect to the existing literature this paper focuses on the complex multi phase fluid dynamics of the sand-air flow, in particular in presence of natural (e.g

dunes) or human-built (e.g. barriers) artifacts, and on deducing a model that includes the mutual interaction of sand, air and obstacles. Sand concentration in the air and the velocity of particles are model's outcomes. This allows to evaluate the transport of sand even where suspension mode is crucial, for instance in presence of a barrier. In these situations the already available models can not be used due to the fact that they solve transport of sand at ground level, or inside a thin layer close to the ground, and therefore they can not evaluate how much sand is entrained in the air and how much of this sand, carried by the wind, overcomes the obstacle.

Referring to [10] for a deeper review of the literature mainly focusing on fluid-dynamic aspects of windblown particulate transport, a first division of the mathematical models for windblown sand can be done distinguishing between Eulerian-Lagrangian and fully Eulerian models. In fact, in both approaches air flow is treated using a continuum model, then working in an Eulerian framework, even though different models have been proposed, e.g. RANS with both 1-equation turbulence closure [11] and 2-equations models [12, 13, 14], LES [15, 16, 17], and lattice-Boltzman approach [18]. On the other hand, regarding the solid phase, the former approach treats each sand particle as a discrete element following it during its trajectories. A different coupling degree can be achieved by including different levels of interaction between particles and air, that can also include how the flow is affected by the presence of sand, and how the particles interact among themselves through inter-particle collisions. The Lagrangian models also differ in the particle collision model, in the treatment of the particle-bed interaction and in the level of coupling. For instance, in [16] all the possible interactions were modeled using a 4-way coupling discrete element method, while in [19] two particle size distributions (Gaussian and uniform) were considered. Unfortunately, Eulerian-Lagrangian models become computationally unfeasible or at least extremely costly for real environmental applications. In fact, they would require to solve an enormous number of ODEs to compute all sand grain trajectories, jointly with the fluid-dynamics for the air-phase.

A different approach consists in working in the spirit of mixture theory and multiphase flows considering sand as a solid immiscible constituent dispersed in the air and described by mass and momentum balance equations. In this way the structure of the model is fully Eulerian. The first works that tried to explore this modeling approach were [20, 21]. In particular, Alhajraf in [20] used both an Eulerian-Lagrangian and a fully Eulerian approach, concluding that the latter is a right compromise between accuracy and computational time.

The present work extends the model presented in [22], with the aim of taking into account of the main phenomena necessary to describe wind-blown sand

(erosion, transport, deposition), coupling them with a morphodynamic evolution model of the sand surface, including an avalanche model presented in [23]. A crucial role is paid by the erosion condition triggering the entire phenomenon (the interested reader is referred to [24] for a critical comparison of all the laws proposed in the literature done on a statistical basis).

In particular, a special attention is given to the case of flows over inclined surfaces, characterizing not only dunes but also the interaction with other structures, generalizing the experimental relation proposed in [25] to the three-dimensional case. Finally, the comprehensive model is used to fully reproduce sand transport in desertic areas in non-equilibrium conditions, i.e. when the sand-bed surface is constantly changing due to erosion and deposition. This is done both in natural conditions, like in presence of dunes, and in presence of human built obstacles.

Dune evolution can be considered as the reference test case of interest because it involves all the physical phenomena that contribute to sand transport together with the aerodynamics of a bluff body in the atmospheric boundary layer. For this reason it was selected here to show the capability of the model to resemble the morphology of dune as final result of the windblown transport process simulated.

As we said above, dune dynamics has been already studied by different authors, from both the pure aerodynamic [26, 27, 28, 29, 30, 31], and the morphodynamic point of view with different focusing: continuous models [5, 32, 9], barchans [33, 34, 35], parabolic and coastal dunes [36, 37], martian dunes [38], linear dunes [39], instabilities [40], star dunes [41, 42] and erosion [43, 14].

Based on the work of Kroy et al. [5], Parteli et al. [44] proposed a three-dimensional model which is able to reproduce shape evolution of different type of dunes. In these works, the separation bubble generated by the dune is heuristically added in the lee, neglecting shear stress and sand fluxes in these region as first approximation, making the model not directly applicable in different situations of interest, for instance in presence of obstacles [45, 46, 47]. In fact, even in the case of a transverse dune, wind flow in the wake is highly non-linear and requires to be carefully solved (see [31] where the effects of boundary conditions on the shear stress patterns in the lee side of a transverse dune are analyzed). Moreover, sand transport and morphological evolution simulations in presence of different sand mitigation measures (see [48] for an exhaustive list) would require at least an apriori knowledge of the flow features, which anyway will introduce a significant approximation on the primary cause of transport, i.e. the wind. Differently, Zhou et al. [49] performed a three-dimensional numerical simulation of a downsized dune migration, based on wall shear stress calculation obtained from LES

simulation. However, even though they computed erosion/deposition based on wall shear stress, they did not explicitly solve suspension and saltation transport, but they only focused on the dune migration, solving an evolution equation of the ground terrain.

Dune migration was also simulated using *Cellular Automaton* algorithms with erosion, transport and deposition phenomena treated using time-dependent stochastic interactions between cells of a lattice [50, 51, 52, 53]. These models are useful in order to study long-term evolution of dune fields, but their aim is not to accurately compute local windblown sand transport, especially in presence of obstacles. In fact, as the above models, the transport is solved at ground-level, i.e. the sand flux is a quantity defined on the ground which account for all the mass transport above in the air. This point is crucial when the wind profile and flow patterns induced by the presence of bluff bodies in the Atmospheric Boundary Layer require to be accurately simulated, and when the assessment of sand particles entrained and transported in the air is the main purpose. For instance this is the case of sandy-wind around sand mitigation measures [45, 54, 55, 56, 57, 46, 47, 48]. In particular, the flow patterns induced are able to entrain particles and to transport them with saltation and suspension modes. This work is intended to present a model capable to reproduce windblown transport also in such situations.

The paper is then organized as follows. First, in Section 2 the mathematical model for both phases is presented with particular attention to the derivation of the evolution equation for the bed level surface and its coupling with the avalanche model. Section 3 is devoted to simulation: first of all the model is tested with a two-dimensional case of a transverse dune and a three-dimensional simulation of evolution of a sand pile from an initial symmetric Gaussian to a barchan-like shape. Having verified the model behavior in these well known configurations, a simulation of windblown sand around a vertical wall is reported, together with other examples of particles transport around different sand mitigation measures, in order to show the area of applications of our study.

Attention is paid to the effects of the dependence of the law of erosion on the slope, on the description of the wind flow patterns around the artifacts and on the mutual interaction wind-sand obstacles. A final section draws some conclusions and remarks.

2. Mathematical modeling

Sandy-wind is modeled as a multiphase-system constituted by the air (the carrying phase) and sand (the dispersed phase). Regarding the former, Atmospheric

Boundary Layer (ABL) flows require the modeling of an unsteady incompressible, turbulent flows. For the considered physical problem and applications, we are interested in the long-time behavior of sand transport, which is mainly due to mean wind flux because sand mass transport occurs at a much longer time scale than turbulence characteristic time scales. For this reason, we model the air-phase using Unsteady Reynolds Averaged Navier-Stokes equations (URANS) coupled with the Shear Stress Transport (SST) formulation of k-ω turbulence model [58, 59] to close the system of equations. With respect to k-ϵ models, k-ω SST performs better in presence of flow separation and adverse pressure gradients ([60]).

We mention that the Reynolds Averaged approach with the selected turbulence model has already been used for dune aerodynamics analysis in [29, 31], and for bluff-body aerodynamics in deserts in [47]. The complete set of equations reads:

$$\begin{cases} \nabla \cdot \overline{\mathbf{u}}_f = 0 \\ \dfrac{\partial \overline{\mathbf{u}}_f}{\partial t} + \overline{\mathbf{u}}_f \cdot \nabla \overline{\mathbf{u}}_f = -\dfrac{1}{\hat{\rho}_f} \nabla \overline{p} + \nabla \cdot \left[(\nu_f + \nu_t) \nabla \overline{\mathbf{u}}_f \right] \\ \dfrac{\partial k}{\partial t} + \nabla \cdot (k \overline{\mathbf{u}}_f) = \nabla \cdot [(\sigma_k \nu_f + \nu) \nabla k] + \tilde{P}_k - \beta^* k \omega \\ \dfrac{\partial \omega}{\partial t} + \nabla \cdot (\omega \overline{\mathbf{u}}_f) = \nabla \cdot [(\sigma_\omega \nu_f + \nu) \nabla \omega] + \alpha \dfrac{\omega}{k} P_k - \beta \omega^2 + (1 - F_1) \dfrac{2 \sigma_\omega}{\omega} \nabla k \cdot \nabla \omega \end{cases} \tag{1}$$

where $\hat{\rho}_f$ is the air density, $\overline{\mathbf{u}}_f$ the averaged fluid velocity, $\overline{p}$ the averaged pressure, k is the turbulent kinetic energy, ω its specific dissipation rate, ν_f the kinematic viscosity, and ν_t the so-called turbulent kinematic viscosity. The kinetic energy production term $\tilde{P}_k$ is modeled by introducing a production threshold to prevent the build-up of turbulence in stagnation regions:

$$\tilde{P}_k = \min\left(P_k, 10\beta^* k\omega\right) \quad \text{being} \quad P_k \approx 2\nu_t \mathbf{D} \cdot \nabla \overline{\mathbf{u}}_f \,,$$

where $\mathbf{D} = \frac{1}{2}(\nabla \overline{\mathbf{u}}_f + \nabla \overline{\mathbf{u}}_f^{\mathrm{T}})$ is the strain rate tensor. For sake of conciseness, the definition of the blending function F_1 and the values of the model constants are omitted herein, but can be found in [59].

The dispersed phase is considered as a passive scalar modelled by the conservation equation for sand volume fraction ϕ_s:

$$\frac{\partial \phi_s}{\partial t} + \nabla \cdot \mathbf{q} = 0 \,, \tag{2}$$

where the flux $\mathbf{q}$ is the combination of advection by wind, sedimentation effects, and diffusive flux due to random collisions:

$$\mathbf{q} = \mathbf{u}_{tr}\phi_s + \mathbf{u}_{sed}\phi_s - \nu_{eff}\phi_s^{k-1}\nabla\phi_s \ , \tag{3}$$

with $k \geq 1$. $\mathbf{u}_{tr}$ is the transport velocity of the solid constituent induced by wind (the advection field), $\mathbf{u}_{sed}$ is the vertical component of velocity due to gravity and ν_{eff} is an effective viscosity. It can be noticed that the order of magnitude of the saltation layer on a flat plane is given by the ratio ν_{eff}/u_{sed}.

As far as the effect of the wind is concerned, following the discussion in [22] and [61], $\mathbf{u}_{tr}$ is taken to be proportional to wind velocity $\mathbf{u}_f$, according to experimental data.

As stated in [22] the settling velocity can be obtained by plotting the experimental relationship between particle Reynolds number and drag given for instance in [62] in terms of a relationship between the grain size and the particle Reynolds number $Re_p = \frac{u_r d}{\nu_f}$, where u_r is the particle sedimenting velocity and d is the particle diameter (see also [63, 64, 65]).

Finally, through the effective viscosity ν_{eff} the last term takes into account of the mixing-diffusive contribution due to the air viscosity ν_f, to the turbulent viscosity ν_t and to the random collisional-interactions ν_s. In [22] it is shown that $\nu_s = \nu_s(I\!I_{\mathbf{D}})$, where $I\!I_{\mathbf{D}}$ is the second invariant of the rate of strain tensor $\mathbf{D}$. In particular, we take $\nu_s = A(2\sqrt{I\!I_{\mathbf{D}}})^{\beta}$, where A and β are model parameters. This formulation implies that ν_s is an objective function, i.e. it does not depend on the reference frame.

2.1. Boundary conditions with slope effects

As already mentioned, one of the crucial mechanisms in sand transport, actually the triggering one, is erosion. In fact, it quantifies the amount of sand entrained by the wind. The phenomenon has been studied from the experimental point of view by several authors (see for instance [2, 66]) and the difference between the proposed laws has been studied in detail in [24]. From the mathematical point of view this phenomenon enters the model as a boundary condition to be applied at the sand-bed to solve the dispersed phase equation.

As already mentioned, erosion occurs if the wall shear stress at the boundary is larger than a threshold value. Otherwise, the boundary condition is $\nabla\phi_s \cdot \mathbf{n} = 0$, which means that no diffusive flux is present and the total outgoing sand-flux is the advective one: $\phi_s(\mathbf{u}_s + \mathbf{u}_w) \cdot \mathbf{n}$.

Otherwise, one has an influx that depends on the difference between the shear stress and a threshold value. For instance, the vertical flux expression obtained by Ho et al. [67, 68, 69] by experiments on saltating grains writes:

$$-\nu_{eff}\phi_s^{k-1}\nabla\phi_s\cdot\mathbf{n} = A_H\hat{\rho}_f\sqrt{\frac{d}{g}}(u^{*^2}-u_t^{*^2})_+\,,$$

where A_H depends on physical properties of the sand and $(f)_+ := (f+|f|)/2$ stands for the positive part of f. In this expression the shear velocity u^* is used instead of the wall shear stress $\boldsymbol{\tau}$. It is defined as $u^* = \sqrt{\frac{|\boldsymbol{\tau}|}{\hat{\rho}_f}}$.

However, as reported in [70], the influence of the slopes on the friction velocity is not negligible. In fact, gravity acts for or against erosion, according to the wind flow direction and the surface slope. In order to include such an effect the following empirical modification was proposed in [25] for two-dimensional problems:

$$u_t^* = u_{t,0}^*\sqrt{\cos\vartheta+\frac{\sin\vartheta}{\tan\theta_{cr}}} = u_{t,0}^*\sqrt{\frac{\sin(\vartheta+\theta_{cr})}{\sin\theta_{cr}}}\,, \tag{4}$$

where $u_{t,0}^*$ is the friction velocity on a flat plane, ϑ is the local inclination of the surface, and θ_{cr} is the repose angle. With this modification that holds for $\vartheta\in[-\theta_{cr},\min\{\theta_{cr},\pi-\theta_{cr}\}]$ the threshold velocity u_t^* amplifies uphill, while it is reduced downhill vanishing when the downhill angle is equal to θ_{cr}, i.e. $\vartheta=-\theta_{cr}$.

The relationship can be generalized to three-dimensional problem assuming that the lifting mechanism is affected by the dynamics in the vertical plane containing the local direction of the wall shear stress

$$\boldsymbol{\tau} = 2\mu[\mathbf{Dn}-(\mathbf{n}\cdot\mathbf{Dn})\mathbf{n}] = \mu\frac{\partial\mathbf{u}_{//}}{\partial\mathbf{n}} = \mu\mathbf{n}\cdot\nabla\mathbf{u}_{//}$$

where $\mathbf{u}_{//}$ is the component of the velocity parallel to the sandbed. Hence, the effective impinging angle to be used in (4) is given by

$$\sin\vartheta = \hat{\boldsymbol{\tau}}\cdot\hat{\mathbf{k}}\,,\quad \hat{\boldsymbol{\tau}} = \frac{\boldsymbol{\tau}}{|\boldsymbol{\tau}|}\,,$$

so that it rewrites as

$$u_t^*(x,t) = u_{t,0}^*\sqrt{\sqrt{1-(\hat{\boldsymbol{\tau}}\cdot\hat{\mathbf{k}})^2}+\frac{\hat{\boldsymbol{\tau}}\cdot\hat{\mathbf{k}}}{\tan\theta_{cr}}}\,. \tag{5}$$

Notice that if $\boldsymbol{\tau} \cdot \hat{\mathbf{k}} = 0$, that is for instance the wind flows along a transverse dune, then $\vartheta = 0$, so that the threshold velocity is the same as for a flow over a flat plane. If, instead, for instance the wind blows perpendicularly to the axis of a transverse dune, then $\boldsymbol{\tau} \cdot \hat{\mathbf{k}}$ is the sine of the slope of the transverse dune and Eq. (4) is recovered.

2.2. *Evolution of the sand-bed surface: Erosion, sedimentation, and avalanches*

Erosion and sedimentation phenomena continuously alter the shape of the sand-bed surface. From the modelling point of view this means that the turbulence equations (1) and the equations for the solid phase (2) have to be integrated in a time-dependent domain and one needs to provide an evolution equation for the free-boundary that will be in charge of describing the morphological changes. From a computational point of view, the new ground configuration is also used to compute ground displacement field to be applied by a front tracking approach and then mesh deformation.

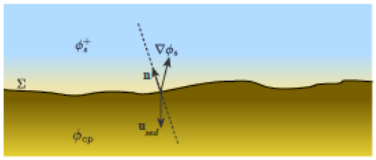

Figure 2: Sand bed interface scheme.

In order to obtain an evolution equation for the sand bed surface, it is sufficient to require continuity of sand flux across the non-material interface Σ which represents the ground level:

$$[\![(\mathbf{q} - \phi_s \mathbf{v}_\Sigma^{ED}) \cdot \mathbf{n}]\!] = 0\,,$$

where $\mathbf{v}_\Sigma^{ED}$ is the descended or ascend velocity due to erosion or sedimentation.

Whence,

$$[\![(\mathbf{u}_{tr}\phi_s + \mathbf{u}_{sed}\phi_s - \nu_{eff}\phi_s^{k-1}\nabla\phi_s - \phi_s \mathbf{v}_\Sigma^{ED}) \cdot \mathbf{n}]\!] = 0\,.$$

Bearing in mind that on the sand-bed side $\mathbf{u}_{tr}^- = \mathbf{u}_{sed}^- = 0$, $\phi_s^- = \phi_{cp}$, the close-packing volue ratio, one has

$$(\mathbf{u}_{tr}\phi_s^+ + \mathbf{u}_{sed}\phi_s^+ - \nu_{eff}(\phi_s^+)^{k-1}\nabla\phi_s^+ - \phi_s^+ \mathbf{v}_\Sigma^{ED}) \cdot \mathbf{n} = (-\phi_{cp}\mathbf{v}_\Sigma^{ED}) \cdot \mathbf{n}\,.$$

Reorganizing and dropping + indices finally gives:

$$\mathbf{v}_{\Sigma}^{ED} \cdot \mathbf{n} = -\frac{1}{\phi_{cp} - \phi_s}(\phi_s \mathbf{u}_{tr} + \phi_s \mathbf{u}_{sed} - \nu_{eff}\phi_s^{k-1}\nabla\phi_s) \cdot \mathbf{n} = D + E\,, \tag{6}$$

where

$$D = -\frac{\phi_s(\mathbf{u}_{tr} + \mathbf{u}_{sed}) \cdot \mathbf{n}}{\phi_{cp} - \phi_s}\,,$$

and

$$E = \frac{\nu_{eff}\phi_s^{k-1}\nabla\phi_s \cdot \mathbf{n}}{\phi_{cp} - \phi_s}\,,$$

are respectively named deposition and erosion velocity. Typically the former is positive and the latter is negative. If deposition prevails on erosion, then the bed-surface velocity is along the normal, which means that the ground level rises. On the contrary, if erosion supersedes, then the ground level lowers down.

We recall that in principle, sand grains can also move and roll along the sand-bed surface contributing to the redistribution of mass and therefore to its evolution of the sand. This is due to creep, raptation and avalanching. Creep and reptation contributions have been included in other works (for instance [49], where reptation flux is proportional to saltation flux, while creep is function of u_*). However, for big amounts of mass transport, the contributions on morphological evolution of the ground surface due to these phenomena are negligible compared with saltation and avalanching and for these reasons they are not considered here and in most of the literature.

Regarding avalanching, the sliding of sand grains is triggered when the slope of the accumulated (or eroded) sand exceeds a critical angle of repose θ_{cr}, which in the case of dry sand is approximately 32°-34°. In light of the application of sand transport in the desert and in particular to dune dynamics, avalanching locally acts to modify slightly supercritical configurations formed by the transfer of sand eroded from upwind locations and deposited on the downwind side of the dune. Neglecting avalanching would then lead to unphysical configurations.

In [23] the authors have derived a mechanical-based model called Degenerate Parabolic Sliding Model (DPSM) for sand slides, providing several numerical simulations with different boundary conditions as well as validation with experimental results from different authors. The evolution equation for the sand bed surface height h reads as:

$$\frac{\partial h}{\partial t} = \nu_{av}\nabla \cdot \left[\frac{(|\nabla h| - \mathrm{tg}\,\theta_{cr})_+}{\sqrt{1 + |\nabla h|^2}}\,\frac{\nabla h}{|\nabla h|}\right], \tag{7}$$

where ν_{av} is related to the adhesivity properties of the particular granular material considered and determines the sliding time of the avalanches, once they are triggered. The square parenthesis on the r.h.s. contains the positive part of a function of the unknown that acts as a trigger of the avalanche flux and then for the evolution of the sand profile.

Including the erosion-deposit contribution $\mathbf{v}_\Sigma^{ED} \cdot \mathbf{n}$ to Eq. (7) one gets the complete evolution equation for h:

$$\frac{\partial h}{\partial t} = \nu_{av} \nabla \cdot \left[\frac{(|\nabla h| - \mathrm{tg}\,\theta_{cr})_+}{\sqrt{1 + |\nabla h|^2}} \frac{\nabla h}{|\nabla h|} \right] + D + E\,, \tag{8}$$

which is a modified Exner equation [71], a sediment mass balance equation developed for river morphology.

3. Numerical simulations

In this section we test the complete transport model in three different cases:

1. The motion of a two dimensional transverse dune.
   This classical case was selected to verify if the model accurately reproduces the main transport processes which lead to the advancement of a transverse dune.
2. Evolution of a sand pile into a Barchan.
   This configuration was selected to verify if the simulated transport process in a three-dimensional domain is able to lead to a coherent evolution of a pile into a barchan. In particular, in this case the generalized formula (5) for u_t^* is used in order to take into account of the effective angle between wind and the local steepest slope direction.
3. Windblown sand transport hindered by a vertical wall and interaction with other obstacles.
   This last case was selected to show the applicability of the model in cases presenting non-standard boundaries. In particular, these cases are significant because they show that the model is capable to face situations of civil engineering interest in which suspension transport becomes crucial, and air-sand interaction is not straightforward and playing a central role in sand transport mechanism so that it needs to be explicitly simulated.

The simulations have been performed on a 10 processors-cluster. Two-dimensional and three-dimensional dunes simulations require two and 4 days respectively.

Specifically focusing on performance, in [72] the authors have recently developed a scheme to accelerate considerably such kind of numerical simulation adapting the discretization time according to the local features of the flow, by means of an ad-hoc domain decomposition method. The numerical scheme has been studied both from accuracy and stability points of view.

3.1. Two-dimensional transverse dune

As a first case, we considered a classical set-up in order to qualitatively test the complete erosion-transport-sedimentation-avalanching model with a well-know configuration already studied with dedicated models (for instance [5, 9]). In fact, we will focus on sand transport around a two dimensional dune (representing a section of an eolian transversal dune) and its migration. As already stated, this is a reference test case of interest because it involves all the physical phenomena contributing to sand transport together with the aerodynamics of a bluff body in the atmospheric boundary layer. With respect to previous studies, we focus on fluid dynamic behavior of the multiphase flow, and in particular on the coupling between air and sand transport, rather than on the long term evolution of the dune.

In this set-up the movement is the result of mass transfer from the soil to the air and then back to the soil. In fact, dune translation is the final effect of the interaction of different phenomena as schematized in Fig.3. The incoming wind reaching the upwind face of the dune accelerates while approaching the crest. Consequently, it applies a growing shear stress on the sand surface, increasing the number of saltating particles and therefore erosion. Overcoming the crest, sand grains arrive in an air recirculation zone, in which the wind is much less energetic, and it does not exert a sufficiently strong shear stress to trigger erosion on the leeward side of the dune and to keep bigger grains entrained in the flow. Therefore, particles deposit starting from the region closer to the crest on the downwind side, that is also characterized by the presence of a stagnation point. Sand then progressively accumulates and when the slope exceeds the critical repose angle, mass slides down forming small avalanches that redistribute the mass in a subcritical manner. For this reason this side is also called the slip face. Looking at the global behavior, the overall effect is that the dune moves downwind. We anticipate that the simulation is able to catch all the just mentioned features.

The simulation set-up is sketched in Fig.4. At the inlet we impose a logarithmic law for the mean wind speed profile,

$$\bar{u}_{f,x}(x_0, t) := u_{abl}(z) = U_{ref} \log\left(\frac{z + z_0}{z_0}\right),$$

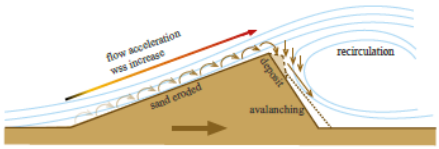

Figure 3: Dune translation motion scheme. Along the upwind face the wind accelerates. Hence, wall shear stress (wss) and therefore erosion increase. Sand deposits in the recirculation zone, also triggering avalanches. As a final result, the dune translates to the right.

and a decreasing exponential profile computed from a steady-state simulation for the sand volume ratio ϕ_s. In addition, for the turbulence quantities k and ω we prescribe Richards and Norris profile [73]. At the outlet, zero-gradient boundary conditions are imposed for all the quantities, except for pressure, which is set to a reference value. At the ground, no-slip condition is used for the velocity.

The aerodynamic roughness of the ground surface is taken into account by using sand-grain roughness wall functions [74] at the ground surface. The equivalent sand grain roughness height is expressed as $k_s = 9.793 z_{0g}/C_s$, where $C_s = 0.5$ is the roughness constant and z_{0g} is the aerodynamic roughness of the ground surface. In [31] the fluid-dynamic model was validated against experimental results for analogous aerodynamic problems.

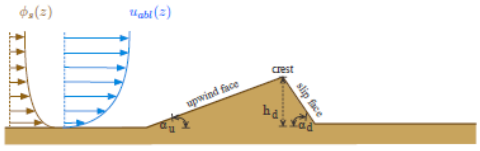

Figure 4: Simulation set-up. The wind blows from left to right. Inlet profiles for ϕ_s and u_f are respectively sketched in brown and blue. The dune reported represents the initial configuration: h_d=1[m], α_u=14^o , α_d=30^o.

At each time step, after solving for both phases, the domain is updated to the new configuration obtained from Eq. (8).

Numerical integration was performed using the finite volume open source code OpenFOAM ®. In particular, in the following we will accurately analyze the simulated results, from both the aerodynamic and the morphodynamic point of view.

In Fig.5 the contour plots of the vertical velocity of sand is reported. Over the upwind face, the velocity points upwards, due to the ramp-effect produced by

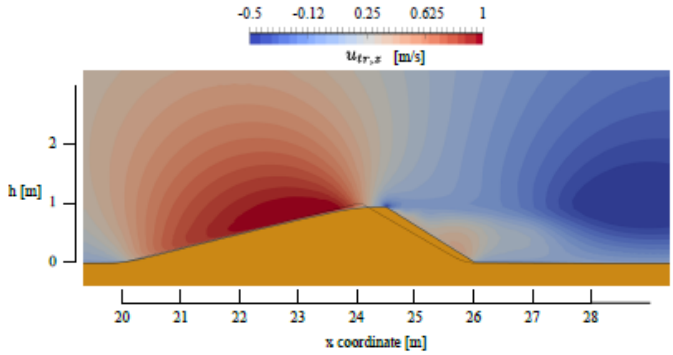

Figure 5: Vertical sand speed contours $u_{s,z}$ at t=600[s]. In black the initial dune shape.

the dune which induces a positive vertical component. The same slightly happens close to slip face too, thanks to the presence of a clockwise recirculation bubble.

Figure 6-a shows the volume ratio ϕ_s close to the dune and the erosion-sedimentation balance v_Σ^{ED} on the sand surface at $t = 600$ [s]. The black line in Figs. 5 and 6 represents the initial dune configuration. The saltation layer is clearly visible and its thickness defined as the height h_s such that

$$\int_0^{h_s} \phi_s(z)dz = 0.95 \int_0^{\infty} \phi_s(z)dz \,, \tag{9}$$

is quantitatively reported in Tab. 1 and is increasing along the dune upwind face.

Position	Saltation layer height [m]
upwind flat zone (before reaching the dune)	0.19
after dune upwind toe	0.24
middle dune upwind face	0.26
close to the crest	0.27

Table 1: Saltation layer thickness at t = 600 [s].

It is worth to point out that, differently from other models (for instance [75]), the saltation layer height is not a model parameter, but it is a result of the balance between diffusion due to particles collision and gravity effect. The same consideration holds for the so-called *saturation length*, studied in [22].

From a morphological point of view, in the upwind region erosion flux is bigger than sedimentation flux, and it has its maximum close to the dune crest (see

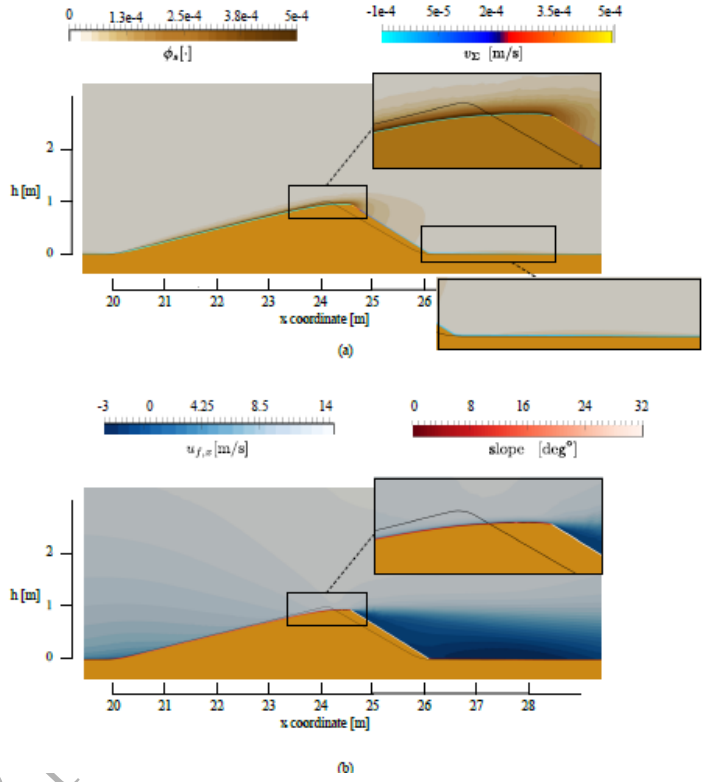

Figure 6: Dune configuration at $t = 600$ [s] (a) volume ration ϕ_s contours (brown) and sand-flux on the ground surface in color; (b) $\bar{u}_{f,x}$ contour and slope of the ground surface. In black the initial dune shape.

the sand-air edge in Fig.6a). It shows the same trend as the saltation layer thickness: the higher the erosion is, the larger the amount of sand entrained by wind is. Looking at the zoomed window on the crest, wind smoothing effect is clearly visible: the initial spiky angle has been flattened due to the increased erosion flux. Moreover, it is interesting to note a thin layer of sand in the air after the slip face (highlighted in the zoomed zone at the bottom in Fig.6a), inside the recirculation zone. This mass is neglected by models in which the recirculation bubble is heuristically placed behind the dune and considering in this zone a negligible shear stress at the ground.

Looking at Fig.6a, on the slip face v_Σ^{ED} is positive, which means that sedimentation is occurring. Sand grains tends to fall and deposit right after the dune ridge. This is due to the fact that this zone corresponds to the wind flow stagnation zone. Progressive accumulation of sand leads to a slope which exceeds the critical one, therefore avalanches can start to lower the slope angle to its repose value $\bar{\theta}$. This is clearly visible in Fig.6b, looking at the slope after the crest, that at $t = 600$ [s] has reached the critical angle of 32^o.

After the slip face, there is a zone in which no saltation occurs. This is due to the fact that there is a recirculation bubble with low wind velocity, visible in Fig.6b, that plots the horizontal component contour of the wind velocity.

To analyze the evolution in time, in Fig.7 the dune profile (yellow-colored), the local slope (blue line) and v_Σ^{ED} (green line) are plotted at different time steps. After 100 [s], the slope has reached the critical value just after the dune crest. This is because in this zone the sedimentation is maximum, as it is a preferential accumulation area where avalanches start forming redistributing the mass downhill, eventually contributing to the advancement of the dune. After about $t = 250$ [s] the entire downwind slope has reached the threshold value and eventually moves as a travelling wave (see also Fig.8). Looking at the last time step, a small accumulation zone is arising at the base of the slip face (it is shown in Figs.6a-b and Fig.5 as well).

Concerning the erosion/deposit phenomenon, it is worth to stress the following aspects:

- far from the dune, both to the left and to the right, there is equilibrium between erosion and deposit, resulting in $v_\Sigma^{ED} \approx 0$;
- approaching the dune, erosion starts to prevail pretty fast and consequently, $v_\Sigma^{ED} < 0$; at $t = 150$ [s] v_Σ^{ED} reaches its minimum just before the sand crest, while after an initial transient, it achieves an almost uniform value along the upwind face;

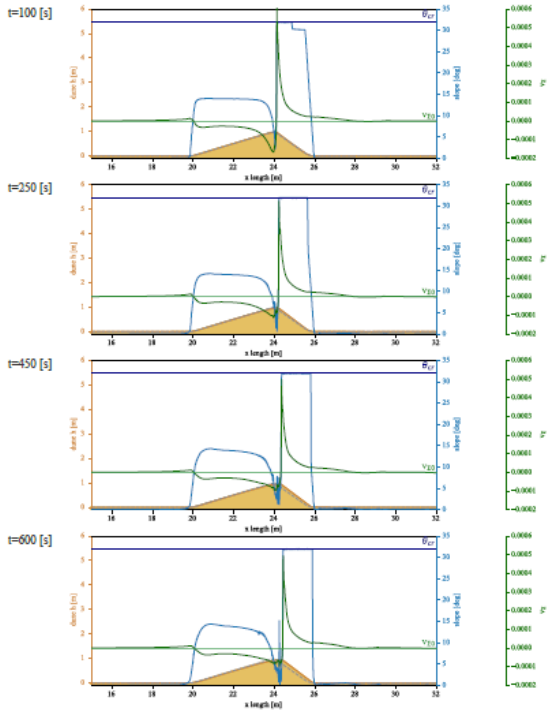

Figure 7: Dune profile (yellow), slope (blue), v_Σ^{ED} (green) at different time steps. Dashed lines represent reference levels: initial dune profile(gray), repose angle (blue), erosion-deposit equilibrium (green).

- crossing the dune crest, there is a jump between erosion and deposition, as expected.

At the brink, sand-bed velocity presents a peak: it comes from the presence of the sharp edge close to the crest, especially at the beginning of the simulation. The peak tends to lower after the initial transient, as the dune approaches a smoother configuration. However, in that zone deposition is maximum because the shear stress goes to zero at the stagnation point.

From $x = 28$ until $x = 29$ is it possible to observe a mild erosion zone (v_Σ^{ED} is negative). As already stated, the details of the phenomenon behind the dune are approximated by models which do not solve the wind flow field.

Finally, in order to look at the phenomena from a global point of view, in Fig.8 the dune crest advancing velocity is plotted. After an initial transient, it looks uniform as predicted from experimental data and simplified models. However,

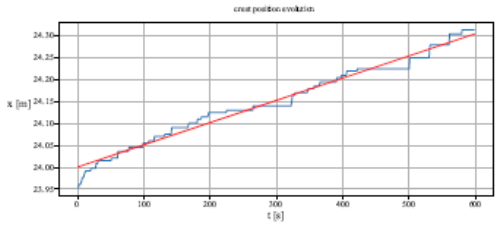

Figure 8: Mean crest position highligthing a nearly constant migration speed after an initial transient of about 20 seconds.

we advice that model parameters have to be tuned in order to match experimental data for real dunes. Only data for much higher dunes are available, therefore for rigorous matching based on migration speed, a simulation with a much larger domain is required.

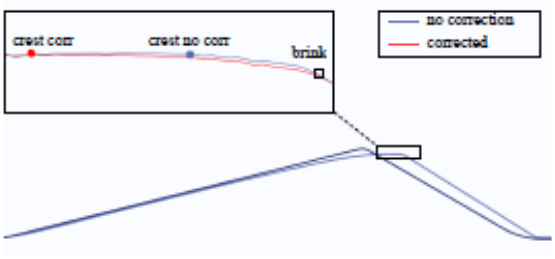

Figure 9: Comparison of the dune configuration at $t = 600$ [s] with and without the slope-sensitive u_t^* model correction, i.e. Eq.(4). The zoomed panel highlights the crest-brink separation obtained using the modified model.

To analyze the influence of the slopes on the friction velocity, i.e. of Eq.(4), we compare in Fig.9 the results of the simulations of the two-dimensional dune with the corrected model and with the slope-independent model. From a global point of view, the behavior is the same. However, some differences can be noted close to the crest of the dune, the zone subject to a fast evolution and to several inclination changes. Looking in detail at the differences, the slope-sensitive modification promotes the crest-brink points separation. This effect is typical of real dunes (see [8, 76]), even if it is almost always neglected in dune aerodynamic studies, which assume idealized triangular shapes. The effect will be bigger in a 3D simulation, because the effective angle ϑ does not vanish in general.

3.2. *Three-dimensional dune simulation: From a symmetric Gaussian pile to a barchan dune*

As a second numerical test we selected a three-dimensional case, using (5), to correct the evaluation of u_t^*. As we mentioned in the introduction, this kind of case have been object of dedicated models (e.g. [33, 34, 35, 49]). The initial sand pile surface is a symmetric Gaussian represented in Fig.10, with maximum height $h_M = 0.5$ [m], a set-up similar to that used in [49]. However, as already mentioned in the introduction, that model avoids the explicit computation of sand saltation and suspension, using a simple model to describe the motion of the dune.

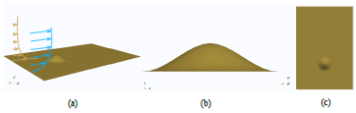

Figure 10: Initial sand-bed configuration for the three-dimensional simulation of a dune. (a) Global view with inlet profiles; (b) horizontal section; (c) top-view.

This kind of dunes are also known as *downsized crescent-shaped dunes*, because the considered sizes are typical of wind tunnel-scale crescent-shaped bedforms (see, for instance, [77] (subaqueous barchans), [78, 79, 70, 80]). The herein used dune size is too large to be reproduced in most of existing wind tunnels, and is closer to real dune size (the minimal size of observed barchan is 1 [m], [81, 77, 79]) observed in desertic areas subject to an almost persistent wind direction.

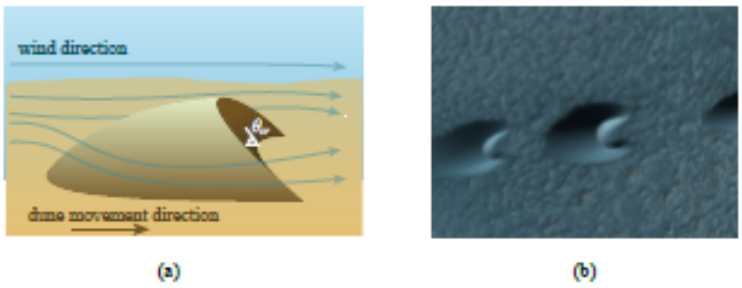

Figure 11: (a) Barchan dune sketch, (b) barchan dunes on Mars (from Wikipedia).

Concerning the simulation set up, the same boundary conditions as for the two-dimensional simulation were used, while for lateral boundary surfaces, symmetry

conditions were imposed.

The transport mechanism and translation are the same reported in Figure 3 for the two-dimensional case, even if three-dimensional wind effects play a crucial role in the particular shape assumed by the sand pile. In fact, under the action of the wind, the shape is modified, tending to a barchan crescent-shaped dune presenting a steep downwind face, with two *horns* pointing downwind as sketched in Figure 11a.

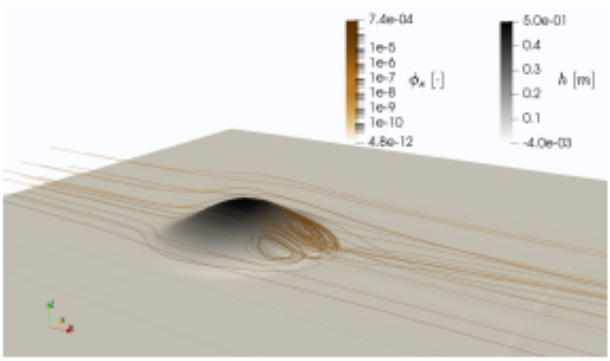

Figure 12: Streamlines around the dune at t=80 [s], colored based on sand volume fraction ϕ_s. In the wake and on the lateral sides, the wind is not directed along the local steepest-slope direction of the surface, therefore it feels an effective angle which is different form the local slope of the surface. The sand surface is colored according to the height (gray scale).

Zhou et al. [49] used the modification for u_t^* reported in Eq. (4), proposed by [25], which does not take into account the effective angle between wind direction and sand surface as done in (5). Of course, as shown in Fig. 12 that shows the streamlines around the dune at t=80 [s], in this case the streamlines close to the pile-surface are not parallel to the steepest slope direction, so that the correction (5) should be used in order to get more accurate results.

Figure 13 compares the initial sand pile shape with the state reached after 145 [s]. The evolution of the shape is a slow process, and the larger the dune, the slower the evolution velocity. Having this in mind, Fig.13-b should be compared with Figure 7-b in [79], which shows the experimental top view of a 20-cm height sand pile evolution.

The surface velocity $\mathbf{v}_\Sigma^{ED}$ contours reported in Figure 14 well explain how this process leads to this particular shape. The sand is eroded from all over the upwind face, and the deposit is maximum at the crest, with a "c"-profile, which forms two

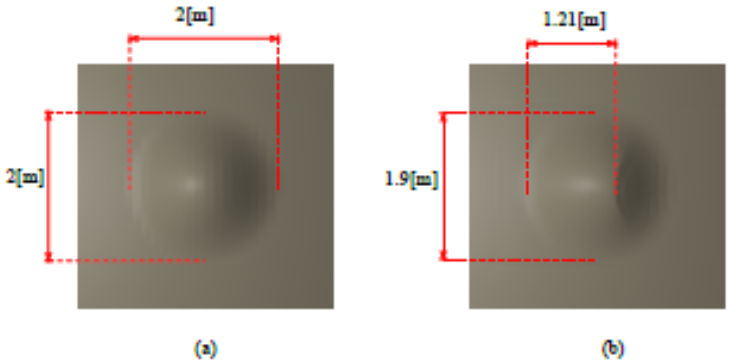

Figure 13: Top view of the initial sand pile (a) and shape after 145 [s] (b)

symmetric preferential directions for avalanche flux, leading to the typical horns of barchan dunes. Moreover, the lateral parts of the initial hill are smaller than the center of the gaussian, and the migration velocity of an along-wind longitudinal slice of hill scales with the inverse of the slice's size. Therefore the lateral parts move faster than the crest. Even if the main features of the evolution are well reproduced, the shape assumed at the end of the simulation (145 [s]) is not a stable-equilibrium configuration. The dune height is slightly decreased. A longer simulation time is required to investigate the long term behavior. A dedicated study on this particular application will be addressed in a future work.

3.3. Windblown sand transport hindered by a vertical wall

The last numerical simulation deals with a straight vertical wall that might be used for windblown sand mitigation. If for the previously presented cases other models have been developed (even if they use approximations on the wind flow treatment, especially in the wake of the dunes), in this last part we present situations in which the effective sand transport in the air has to be explicitly simulated by means of a multiphase approach. Such an example is suggested by civil engineering interests in testing such kinds of devices (e.g. [45, 46, 47, 48, 82]). In the same context, at the end of the section we show that the model can be used to simulate other non standard sandy-flows interacting with different obstacles, such as a porous barrier and a ditch.

The vertical wall presents two mains features which can be handled by the proposed model:

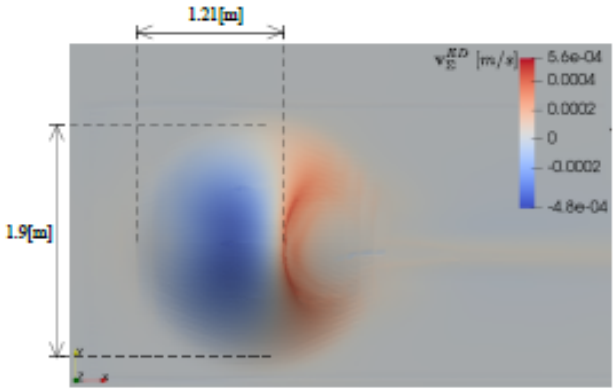

Figure 14: $\mathbf{v}_{\Sigma}^{ED}$ on the sand surface at t=80 [s]. Erosion-deposition fluxes modify the surface which starts to appear similar to barchan shape. In particular the deposition peak immediately after the crest and the linked avalanche surface-flux causes the formation of lateral *horns*.

1. the bluff body induces recirculation bubbles both upwind and downwind (see [47]). Such generated flow structures require the flow to be solved accurately and can not be predicted by perturbation theory. Moreover, the air-flow modeling approach and the turbulence model should be selected accurately. As stated above, k-ω SST turbulence model has been used by different authors for the same class of problem (e.g [29], [47]), and fully validated in [83].
2. The presence of the obstacle makes the already developed models for dune evolution not directly applicable to this case. The complex suspension transport mode is crucial to evaluate the amount of sand trapped by the mitigation measure, the amount of sand overcoming it and where it deposits upwind.

Such a case is analogous to one of the configurations studied in wind tunnel for a particular barrier's shape in [46].

The configuration studied is shown in Figure 15. The barrier is 1[m] high. At the beginning of the simulation an initial amount of sand is placed in front of the barrier, with a straight profile inclined with an angle of about 11^o. Two recirculation bubbles are generated: a bigger one in the wake of the barrier, and a small eddy upwind. The saltation layer is accurately reproduced and reported in Figure 16. As for the barrier studied in [46], the wind-flow digs the sand altering the initial straight profile, as shown in Figure 17, which compares initial and final shapes of the sand pile upwind the barrier. It is interesting to note the mutual effect

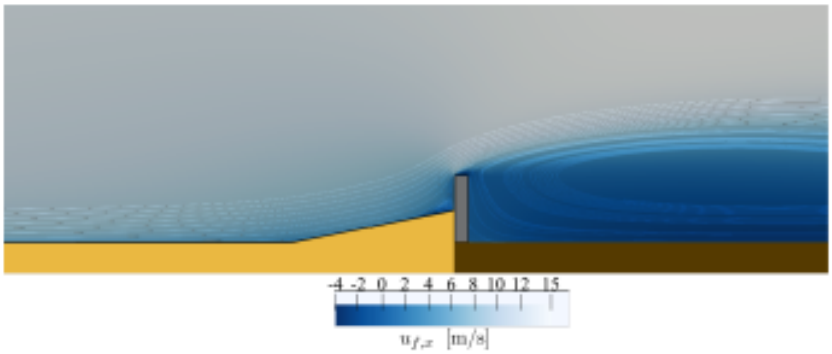

Figure 15: Vertical wall with initial pile of accumulated sand. The sandy terrain is colored in yellow. Brown color indicates the ground sand-free. The horizontal wind velocity field is reported with the streamlines around the barrier.

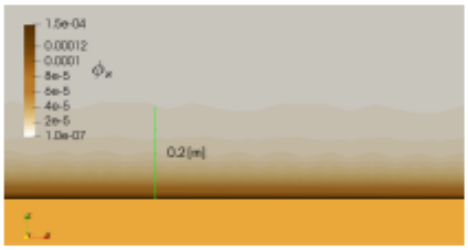

Figure 16: Saltation layer upwind the barrier. Its height evaluated using criterium 9 is about 20 [cm] as commonly observed in reality.

Figure 17: Initial and final sand profile and sand volume ratio around the barrier. The upwind vortex generated by the barrier is altered by the ground evolution.

of wind and sand: the shear stress generated by the upwind vortex is capable to erode a certain amount of sand; this process alters the shape of the sand profile, which consequently affects the shape of the bubble. The profile after 145 [s] shows an analogous modification induced by the upwind vortex observed in wind tunnel for a different barrier [46].

Looking at the final state, it is clearly visible that a certain amount of sand entrained in the air is capable to overcome the wall. From a quantitative point of view, this amount of mass can be obtained integrating along a vertical line the normal sand flux $q_{s,x} = u_{tr,x}\phi_s\hat{\rho}_s$ obtaining the integral sand drift, which can be used to evaluate the efficiency of the barrier as sand mitigation measure.

In the same spirit, other mitigation measures can be studied as the ones reported in Figure 18: a 40%-porous barrier and a ditch. Figure 18 shows the wind velocity magnitude, the turbulent kinetic energy and the sand volume ratio in the air. The porous fence generates complicated flow patterns in the wake that are hard to be approximated and are strongly affected by the porosity [56].

Concerning the ditch shown again in Fig. 18 (bottom row), from a pure aerodynamic point of view, as the sand fills the ditch the size of the vortex inside changes in shape and size, altering the shear stress at the ground and consequently the erosion. Moreover, the presence of an obstacle makes the suspension transport relevant, especially in light of the application for which this artifact is built.

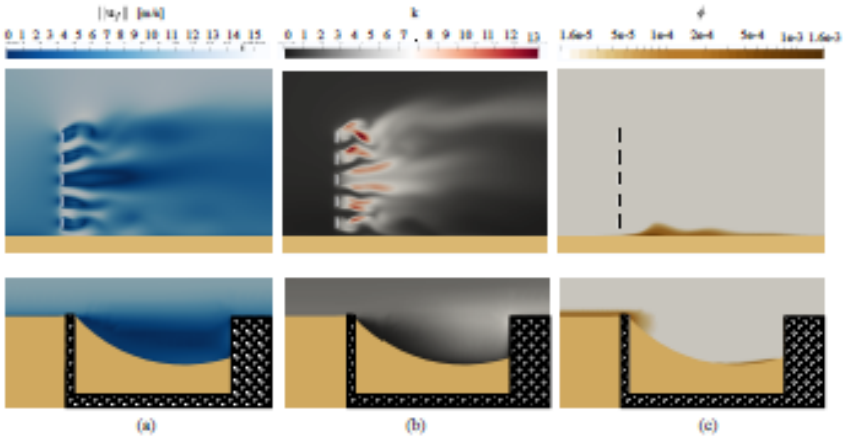

Figure 18: (a) wind velocity magnitude, (b) turbulent kinetic energy, (c) sand volume fraction, for a porous barrier with horizontal slats (first row) and a ditch (second row).

4. Conclusions

The fully Eulerian model proposed in this paper is able to describe the motion of windblown sand in the air and the evolution of sand-bed. It takes into account the main physical phenomena contributing to sand transport at medium-large scale, that is to say, erosion, saltation and suspension transport, sedimentation, and avalanching. In this way it is capable to deal with the morphological changes present both in complex natural phenomena like dune migration dynamics, and in the interactions with built artifacts like obstacles. This feature is particularly interesting for engineering applications when the interaction between sand and infrastructures need be studied. An example is the identification of sand mitigation devices, the evaluation of their efficacy and of the regions where sand accumulates.

The proposed model solves for the wind flow fields, allowing to simulate situations in which complicated flow structures are generated. Moreover, the model explicitly computes the concentration of sand in the air due to suspension transport mode, the interaction of particles among themselves in the saltation layer, the erosion/deposition fluxes and the sliding of grains, resulting in the evolution of the ground surface.

At the cost of an increased complexity of the model, the accuracy of the interaction between the phases could be improved by considering a momentum balance equations for the dispersed phase, both in a monodisperse and in a polidisperse case. This modification might become particularly relevant very close to the ground, where saltation takes place and sand concentration is the highest. Moreover, creep and reptetion bed-flux could be included as well. These improvements can be useful for small scale modeling and simulations.

The same physical laws govern other particulate transport phenomena. With some obvious changes and adaptations, the same modelling approach could be extended to the transport and deposition of other particulate windblown flows, such as snow, rain, and vulcanic ashes.

Acknowledgment

The authors wish to thank L. Bruno, R. Nuca and N. Coste, members of the Windblown Sand Modeling and Mitigation joint research, development and consulting group established between Politecnico di Torino and Optiflow Co., H. Jasak and his research group of Univeristy of Zagreb, for helpful discussions about the topics of the paper. This research was supported in part by the Istituto Nazionale di Alta Matematica and Regione Piemonte. The research activity

was developed within the MSCA-ITN-2016-EID SMaRT research project. This project has received funding from the European Union's Horizon 2020 research and innovation programme (grant agreement No.721798).

References

References

[1] J. Kok, E. Parteli, T. Michaels, D. Karam, The physics of wind-blown sand and dust, Rep Prog in Phys 75 (10) (2012) 106901.

[2] R. Bagnold, The Physics of Blown Aand and Desert Dunes, Methuen & Company, 1941.

[3] R. Anderson, P. Haff, Simulation of eolian saltation, Science 241 (4867) (1988) 820–823.

[4] G. Sauermann, K. Kroy, H. Herrmann, Continuum saltation model for sand dunes, Phys Rev E 64 (3) (2001) 031305.

[5] K. Kroy, G. Sauermann, H. J. Herrmann, Minimal model for aeolian sand dunes, Phys Rev E 66 (3) (2002) 031302.

[6] G. Sauermann, J. Andrade, L. Maia, U. Costa, A. Araújo, H. Herrmann, Wind velocity and sand transport on a barchan dune, Geomorphology 54 (3-4) (2003) 245–255. doi:10.1016/S0169-555X(02)00359-8.

[7] B. Andreotti, A two-species model of aeolian sand transport, J Fluid Mech. 510 (2004) 47–70. doi:10.1017/S0022112004009073.

[8] E. Parteli, V. Schwämmle, H. Herrmann, L. Monteiro, L. Maia, Profile measurement and simulation of a transverse dune field in the lençóis maranhenses, Geomorphology 81 (1-2) (2006) 29–42.

[9] M. Pischiutta, L. Formaggia, F. Nobile, Mathematical modelling for the evolution of aeolian dunes formed by a mixture of sands: entrainment-deposition formulation, CAIM 2 (2).

[10] A. Lo Giudice, R. Nuca, L. Preziosi, N. Coste, Wind-blown particulate transport: A review of computational fluid dynamics models, Mathematics in Engineering (2019) (accepted).

[11] L. Kang, Discrete particle model of aeolian sand transport: Comparison of 2D and 2.5 d simulations, Geomorphology 139 (2012) 536–544. doi:10.1016/j.geomorph.2011.12.005.

[12] L. Kang, L. Guo, Eulerian–lagrangian simulation of aeolian sand transport, Powder Technol 162 (2) (2006) 111–120.

[13] L. Kang, D. Liu, Numerical investigation of particle velocity distributions in aeolian sand transport, Geomorphology 115 (1-2) (2010) 156–171.

[14] A. Lopes, L. Oliveira, A. D. Ferreira, J. Pinto, Numerical simulation of sand dune erosion, Environ Fluid Mech 13 (2) (2013) 145–168. doi:10.1007/s10652-012-9263-2.

[15] D. Tong, N. Huang, Numerical simulation of saltating particles in atmospheric boundary layer over flat bed and sand ripples, J Geophys Res Atmos 117 (D16205).

[16] Z. Li, Y. Wang, Y. Zhang, A numerical study of particle motion and two-phase interaction in aeolian sand transport using a coupled large eddy simulation - discrete element method, Sedimentology 61 (2) (2014) 319–332. doi:10.1111/sed.12057.

[17] H. Jiang, H. Dun, D. Tong, N. Huang, Sand transportation and reverse patterns over leeward face of sand dune, Geomorphology 283 (2017) 41–47.

[18] X. Shi, P. Xi, J. Wu, A lattice Boltzmann-Saltation model and its simulation of aeolian saltation at porous fences, Theor Comp Fluid Dyn 29 (1-2) (2015) 1–20. doi:10.1007/s00162-014-0338-1.

[19] F. Xiao, L. Guo, D. Li, Y. Wang, Discrete particle simulation of mixed sand transport, Particuology 10 (2) (2012) 221–228. doi:10.1016/j.partic.2011.10.004.

[20] S. Alhajraf, Numerical simulation of drifting sand, Phd thesis, Cranfield University (2000).

[21] S. Ji, A. Gerber, A. Sousa, A convection-diffusion CFD model for aeolian particle transport, Int J Numer Meth Fl 45 (8) (2004) 797–817. doi:10.1002/fld.724.

[22] L. Preziosi, D. Fransos, L. Bruno, A multiphase first order model for non-equilibrium sand erosion, transport and sedimentation, Appl Math Lett 45 (2015) 69–75. doi:10.1016/j.aml.2015.01.011.

[23] A. Lo Giudice, G. Giammanco, D. Fransos, L. Preziosi, Modelling sand slides by a mechanics-based degenerate parabolic equation, Math Mech Solids (2018) .doi:10.1177/1081286518755230.

[24] L. Raffaele, L. Bruno, F. Pellerey, L. Preziosi, Windblown sand saltation: A statistical approach to fluid threshold shear velocity, Aeolian Res 23 (2016) 79–91.

[25] J. Iversen, K. Rasmussen, The effect of wind speed and bed slope on sand transport, Sedimentology 46 (4) (1999) 723–731. doi:10.1046/j.1365-3091.1999.00245.x.

[26] D. Parsons, I. Walker, G. Wiggs, Numerical modelling of flow structures over idealized transverse aeolian dunes of varying geometry, Geomorphology 59 (1-4) (2004) 149–164. doi:10.1016/j.geomorph.2003.09.012.

[27] D. Parsons, G. Wiggs, I. Walker, R. Ferguson, B. Garvey, Numerical modelling of airflow over an idealised transverse dune, Environ Model Softw 19 (2) (2004) 153–162. doi:10.1016/S1364-8152(03)00117-8.

[28] V. Schatz, H. Herrmann, Flow separation in the lee side of transverse dunes: a numerical investigation, Geomorphology 81 (1-2) (2006) 207–216.

[29] B. Liu, J. Qu, W. Zhang, G. Qian, Numerical simulation of wind flow over transverse and pyramid dunes, J Wind Eng Ind Aerod 99 (8) (2011) 879–888.

[30] A. Araújo, E. Parteli, T. Pöschel, J. Andrade, H. Herrmann, Numerical modeling of the wind flow over a transverse dune, Sci Rep 3 (2858) (2013) 1–9. doi:10.1038/srep02858.

[31] L. Bruno, D. Fransos, Sand transverse dune aerodynamics: 3D coherent flow structures from a computational study, J Wind Eng Ind Aerod 147 (2015) 291–301.

[32] O. Durán, E. J. Parteli, H. J. Herrmann, A continuous model for sand dunes: Review, new developments and application to barchan dunes and barchan dune fields, Earth Surf Proc Land 35 (13) (2010) 1591–1600.

[33] V. Schwämmle, H. J. Herrmann, Geomorphology: Solitary wave behaviour of sand dunes, Nature 426 (6967) (2003) 619.

[34] V. Schwämmle, H. Herrmann, A model of barchan dunes including lateral shear stress, Eur Phys J E 16 (1) (2005) 57–65.

[35] O. Durán, V. Schwämmle, H. Herrmann, Breeding and solitary wave behavior of dunes, Phys Rev E 72 (2) (2005) 021308.

[36] O. Durán, H. J. Herrmann, Vegetation against dune mobility, Phys. Rev. Lett. 97 (2006) 188001. doi:10.1103/PhysRevLett.97.188001.

[37] O. Durán, L. J. Moore, Vegetation controls on the maximum size of coastal dunes, Proceedings of the National Academy of Sciences 110 (43) (2013) 17217–17222. doi:10.1073/pnas.1307580110.

[38] E. J. R. Parteli, H. J. Herrmann, Saltation transport on mars, Phys. Rev. Lett. 98 (2007) 198001. doi:10.1103/PhysRevLett.98.198001.

[39] E. J. R. Parteli, O. Durán, H. Tsoar, V. Schwämmle, H. J. Herrmann, Dune formation under bimodal winds, Proceedings of the National Academy of Sciences 106 (52) (2009) 22085–22089. doi:10.1073/pnas.0808646106.

[40] E. J. R. Parteli, J. S. Andrade, H. J. Herrmann, Transverse instability of dunes, Phys. Rev. Lett. 107 (2011) 188001. doi:10.1103/PhysRevLett.107.188001.

[41] D. Zhang, C. Narteau, O. Rozier, S. Courrech du Pont, Morphology and dynamics of star dunes from numerical modelling, Nat. Geosci. 5 (7) (2012) 463. doi:10.1038/ngeo1503.

[42] X. Gao, C. Narteau, O. Rozier, S. C. Du Pont, Phase diagrams of dune shape and orientation depending on sand availability, Sci. Rep. 5 (2015) 14677. doi:10.1038/srep14677.

[43] A. Farimani, A. Ferreira, A. Sousa, Computational modeling of the wind erosion on a sinusoidal pile using a moving boundary method, Geomorphology 130 (3-4) (2011) 299–311.

[44] E. J. R. Parteli, K. Kroy, H. Tsoar, J. S. Andrade, T. Pöschel, Morphodynamic modeling of aeolian dunes: Review and future plans, Eur Phys J-Spec Top 223 (11) (2014) 2269–2283.

[45] S. Hotta, K. Horikawa, Function of sand fence placed in front of embankment, in: Coastal Engineering 1990, American Society of Civil Engineers, New York, NY, 1991, pp. 2754–2767.

[46] L. Bruno, N. Coste, D. Fransos, A. Lo Giudice, L. Preziosi, L. Raffaele, Shield for sand: an innovative barrier for windblown sand mitigation, Recent Pat on Eng 12 (3) (2018) 237–246.

[47] L. Bruno, D. Fransos, A. Lo Giudice, Solid barriers for windblown sand mitigation: Aerodynamic behavior and conceptual design guidelines, J Wind Eng Ind Aerod 173 (2018) 79–90.

[48] L. Bruno, M. Horvat, L. Raffaele, Windblown sand along railway infrastructures: A review of challenges and mitigation measures, J Wind Eng Ind Aerod 177 (2018) 340–365.

[49] X. Zhou, Y. Zhang, Y. Wang, M. Li, 3d numerical simulation of the evolutionary process of aeolian downsized crescent-shaped dunes, Aeolian Res 21 (2016) 45–52.

[50] B. Werner, Eolian dunes: computer simulations and attractor interpretation, Geology 23 (12) (1995) 1107–1110. doi:10.1130/0091-7613(1995)023<1107:EDCSAA>2.3.CO;2.

[51] H. Nishimori, M. Yamasaki, A simple model for the various pattern dynamics of dunes, Int J Mod Phys B 12 (03) (1998) 257–272. doi:10.1142/S021797929800020X.

[52] A. Katsuki, H. Nishimori, N. Endo, K. Taniguchi, Collision dynamics of two barchan dunes simulated using a simple model, J Phys Soc Jpn 74 (2) (2005) 538–541.

[53] C. Narteau, D. Zhang, O. Rozier, P. Claudin, Setting the length and time scales of a cellular automaton dune model from the analysis of superimposed bed forms, J Geophys Res Earth Surf 114 (F3). doi:10.1029/2008JF001127.

[54] N. Zhang, J. H. Kang, S. J. Lee, Wind tunnel observation on the effect of a porous wind fence on shelter of saltating sand particles, Geomorphology 120 (3-4) (2010) 224–232.

[55] N. Zhang, S. J. Lee, T. G. Chen, Trajectories of saltating sand particles behind a porous fence, Geomorphology 228 (2015) 608–616.

[56] B. Li, D. J. Sherman, Aerodynamics and morphodynamics of sand fences: A review, Aeolian Res 17 (2015) 33–48.

[57] J. J. Cheng, J. Q. Lei, S. Y. Li, H. F. Wang, Disturbance of the inclined inserting-type sand fence to wind–sand flow fields and its sand control characteristics, Aeolian Res 21 (2016) 139–150.

[58] F. Menter, Two-equation eddy-viscosity turbulence models for engineering applications, AIAA J 32 (8) (1994) 1598–1605.

[59] F. Menter, M. Kuntz, R. Langtry, Ten years of industrial experience with the sst turbulence model, Turbulence, heat and mass transfer 4 (1) (2003) 625–632.

[60] F. Menter, Zonal two equation kw turbulence models for aerodynamic flows, in: 23rd fluid dynamics, plasmadynamics, and lasers conference, 1993, p. 2906.

[61] S. Balachandar, J. Eaton, Turbulent dispersed multiphase flow, Annu Rev Fluid Mech 42 (2010) 111–133.

[62] E. Barnea, J. Mizrahi, A generalized approach to the fluid dynamics of particulate systems: Part 1. General correlation for fluidization and sedimentation in solid multiparticle systems, Chem Eng J 5 (2) (1973) 171–189. doi:10.1016/0300-9467(73)80008-5.

[63] P. Brown, D. Lawler, Sphere drag and settling velocity revisited, J Environ Eng 129 (3) (2003) 222–231.

[64] E. Farrell, D. Sherman, A new relationship between grain size and fall (settling) velocity in air, Prog Phys Geog 39 (3) (2015) 361–387.

[65] G. Bagheri, C. Bonadonna, On the drag of freely falling non-spherical particles, Powder Technol 301 (2016) 526–544.

[66] Y. Shao, H. Lu, A simple expression for wind erosion threshold friction velocity, J Geophys Res Atmospheres 105 (D17) (2000) 22437–22443. doi:10.1029/2000JD900304.

[67] T. Ho, P. Dupont, A. EI Moctar, A. Valance, Particle velocity distribution in saltation transport, Phys Rev E 85 (5) (2012) 052301. doi:10.1103/PhysRevE.85.052301.

[68] T. Ho, A. EI Moctar, P. Dupont, Scaling laws in aeolian sand transport, Phys Rev Lett 106 (9) (2013) 094501.

[69] T. D. Ho, A. Valance, P. Dupont, A. El Moctar, Aeolian sand transport: Length and height distributions of saltation trajectories, Aeolian Res 12 (2014) 65–74.

[70] R. Faria, A. Ferreira, J. Sismeiro, J. Mendes, A. Sousa, Wind tunnel and computational study of the stoss slope effect on the aeolian erosion of transverse sand dunes, Aeolian Res 3 (3) (2011) 303–314. doi:10.1016/j.aeolia.2011.07.004.

[71] F. M. Exner, Uber die wechselwirkung zwischen wasser und geschiebe in flussen, Akad Wiss Wien Math Naturwiss Klasse 134 (2a) (1925) 165–204.

[72] C. Canuto, A. Lo Giudice, A multi-timestep robin-robin domain decomposition method for time dependent advection-diffusion problems, App Math Comput (2018) (under review).

[73] P. Richards, S. Norris, Appropriate boundary conditions for computational wind engineering models revisited, J Wind Eng Ind Aerod 99 (4) (2011) 257–266.

[74] B. Blocken, T. Stathopoulos, J. Carmeliet, Cfd simulation of the atmospheric boundary layer: wall function problems, Atmos Environ 41 (2) (2007) 238–252.

[75] O. Durán, E. Parteli, H. Herrmann, A continuous model for sand dunes: Review, new developments and application to barchan dunes and barchan dune fields, Earth Surf Process Landf 35 (13) (2010) 1591–1600.

[76] G. Sauermann, P. Rognon, A. Poliakov, H. Herrmann, The shape of the barchan dunes of southern morocco, Geomorphology 36 (1-2) (2000) 47–62.

[77] P. Hersen, S. Douady, B. Andreotti, Relevant length scale of barchan dunes, Phys Rev Lett 89 (26) (2002) 264301.

[78] O. Dauchot, F. Lechénault, C. Gasquet, F. Daviaud, "barchan" dunes in the lab, CR Mecanique 330 (3) (2002) 185–191.

[79] B. Andreotti, P. Claudin, S. Douady, Selection of dune shapes and velocities part 1: Dynamics of sand, wind and barchans, Eur Phys J B 28 (3) (2002) 321–339.

[80] Y. Zhang, Y. Wang, P. Jia, Evolution of downsized crescent-shaped dune in wind tunnel experiment, Sci China Phys Mech 57 (1) (2014) 143–151.

[81] S. Hastenrath, The barchan dunes of southern peru revisited, Z. Geomorph. 31 (1987) 167–178.

[82] S. Zhang, G. D. Ding, M. H. Yu, G. L. Gao, Y. Y. Zhao, L. Wang, Y. Z. Wang, Application of boundary layer displacement thickness in wind erosion protection evaluation: Case study of a salix psammophila sand barrier, Intern J Env Res Pub Health 16 (2019) 592. doi:10.3390/ijerph16040592.

[83] L. Bruno, D. Fransos, Sand transverse dune aerodynamics: 3d coherent flow structures from a computational study, J Wind Eng Ind Aerod 147 (2015) 291–301.